Cell

The Native 3D Organization of Bacterial Polysomes

Florian Brandt,[1,2] Stephanie A. Etchells,[2] Julio O. Ortiz,[1] Adrian H. Elcock,[4] F. Ulrich Hartl,[2,3,*] and Wolfgang Baumeister[1,3,*]
[1]Department of Molecular Structural Biology
[2]Department of Cellular Biochemistry
Max Planck Institute of Biochemistry, Am Klopferspitz 18, Martinsried 82152, Germany
[3]Center for Integrated Protein Science Munich, Ludwig-Maximilians-Universität München, Butenandtstr. 5-13, München 81377, Germany
[4]Department of Biochemistry, University of Iowa, 4-530 Bowen Science Building, 51 Newton Road, Iowa City, IA 52242, USA
*Correspondence: uhartl@biochem.mpg.de (F.U.H.), baumeist@biochem.mpg.de (W.B.)
DOI 10.1016/j.cell.2008.11.016

SUMMARY

Recent advances have led to insights into the structure of the bacterial ribosome, but little is known about the 3D organization of ribosomes in the context of translating polysomes. We employed cryoelectron tomography and a template-matching approach to map 70S ribosomes in vitrified bacterial translation extracts and in lysates of active *E. coli* spheroplasts. In these preparations, polysomal arrangements were observed in which neighboring ribosomes are densely packed and exhibit preferred orientations. Analysis of characteristic examples of polysomes reveals a staggered or pseudohelical organization of ribosomes along the mRNA trace, with the transcript being sequestered on the inside, the tRNA entrance sites being accessible, and the polypeptide exit sites facing the cytosol. Modeling of elongating nascent polypeptide chains suggests that this arrangement maximizes the distance between nascent chains on adjacent ribosomes, thereby reducing the probability of intermolecular interactions that would give rise to aggregation and limit productive folding.

INTRODUCTION

Ribosomes are the essential machines of protein synthesis in all cells. Much has been learned in recent years about the structure and function of the bacterial ribosome from crystallography (Ban et al., 2000; Schuwirth et al., 2005; Wimberly et al., 2000) and single-particle analysis by cryoelectron microscopy (Agrawal et al., 2000; Gabashvili et al., 2000; Valle et al., 2003a). Significant progress has been made in understanding the pathway of the synthesized peptide through the exit tunnel of the 50S ribosomal subunit and its interactions with ribosomal components and molecular chaperones (Bashan and Yonath, 2005; Baram et al., 2005; Hsu et al., 2007). In contrast, little is known about the spatial arrangement of individual ribosomes in the context of polysomes during active protein synthesis.

Linear polysomal arrays of translating ribosomes were first observed in reticulocyte translation lysates by sedimentation analysis and conventional transmission electron microscopy (TEM) (Warner et al., 1962). Various polysome arrangements have been described from TEM micrographs of mammalian and bacterial cells (Rich, 1963; Slayter et al., 1968; Staehelin et al., 1963). More recently, wheat germ polysomes formed in vitro have been reported to adopt ordered structure (Kopeina et al., 2008; Madin et al., 2004). However, the preparation methods of metal shadowing or negative staining used previously may be prone to artifacts. In contrast, cryoelectron microscopy (cryo-EM) single-particle analysis avoids the staining and dehydration problems but requires essentially repetitive structures, a prerequisite not met by supramolecular assemblies such as polysomes. Moreover, two-dimensional TEM projections do not per se provide insight into the three-dimensional (3D) organization of molecular assemblies.

Cryoelectron tomography (CET) overcomes these limitations and allows us to obtain a 3D model of native polysomes into which the high-resolution map of the ribosome can be docked. CET is a powerful method to reconstruct the 3D electron densities of individual macromolecular objects in a close-to-native environment without the need to stain or fix the specimen (Lucic et al., 2005). A comprehensive interpretation of tomograms is achieved by pattern recognition based on crosscorrelation between a known high-resolution structure and target structures in the tomogram, as demonstrated with macromolecular complexes enclosed in phantom cells (Bohm et al., 2000; Frangakis et al., 2002). At present, however, the application of this method to intact cells is limited due to the low signal-to-noise ratio of cellular tomograms, particularly when working with prokaryotic cells exceeding 0.5 μm in thickness. Although, in thin, intact cells, CET allows the determination of coordinates and orientations of large complexes, such as 70S ribosomes, at an intermediate resolution of 4–5 nm (Ortiz et al., 2006), an unambiguous identification of individual polysome structures is hard to achieve due to the crowding of these systems. Since the analysis of polysome organization requires the reliable localization and correct identification of individual ribosomes bound to the same mRNA, we decided to work with actively translating cell lysates or *E. coli* spheroplast lysates in order to achieve

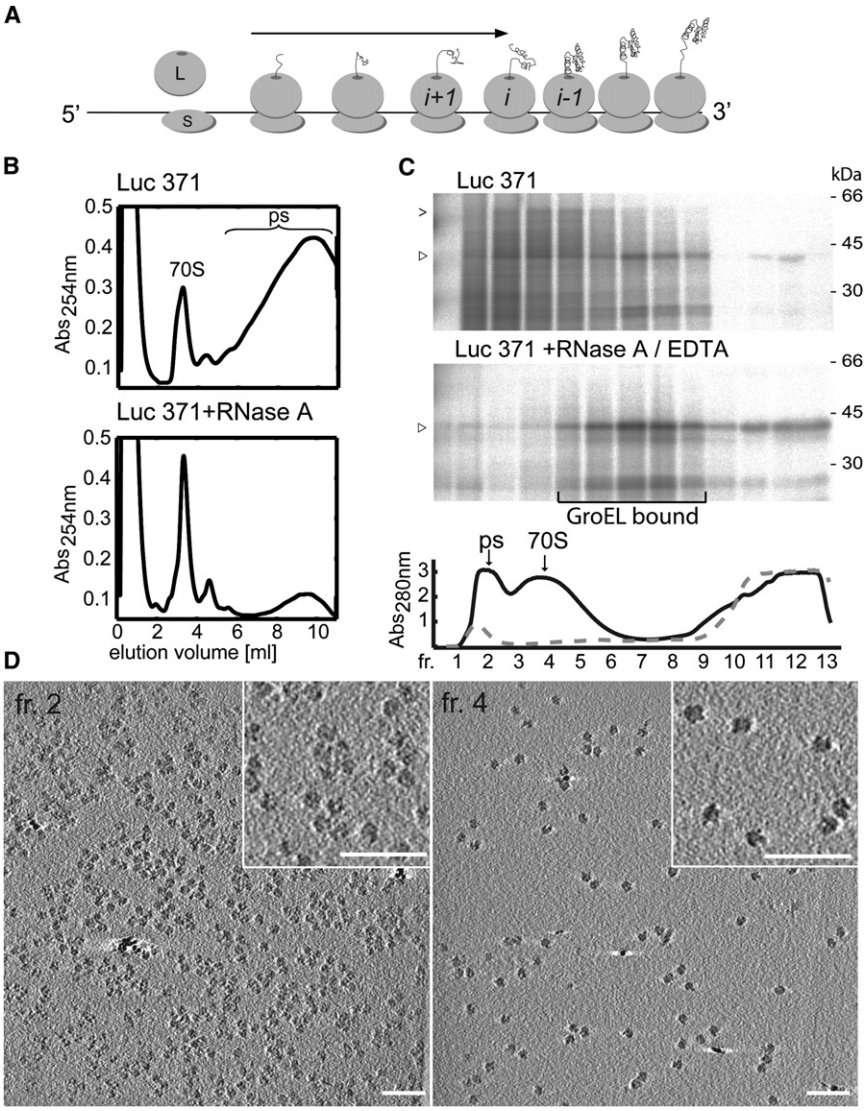

Figure 1. Polysome Formation In Vitro

(A) Linear schematic for polysomal assemblies with indices (*i*, *i+1*…), as used in the text. (L, S) Large, small ribosomal subunit. (Black line) mRNA. Growing nascent peptides are indicated in black.

(B) In vitro translation reactions of Luc 371 were resolved by sucrose gradient centrifugation and the absorption profile recorded at 254 nm without or with prior RNase A treatment. Positions of 70S ribosomes and polysomes (ps) are indicated.

(C) Size exclusion chromatography of samples as in (B) followed by SDS-PAGE of eluted fractions. The p-tRNA containing stalled nascent chain species are indicated by an arrowhead, while the hydrolyzed nascent chains are indicated by a closed arrowhead. The absorption profile at 280 nm is shown (solid line, without RNase A/EDTA; dashed line, with RNase A/EDTA). The fractionation of GroEL-associated Luc 371 chains is indicated.

(D) Tomographic reconstructions of vitrified fraction 2 (polysomes) and fraction 4 (monosomes as well as small polysomes) as prepared in (C). Inserts show magnified views. Scale bars, 100 nm.

a better spatial separation of individual polysomes. Once the structural characteristics of polysomes are established, this information can be used to interpret in situ images of polysomes or other supramolecular ribosome assemblies.

Here, we provide a 3D description of bacterial polysome structures, demonstrating the occurrence of polysomes with densely packed neighboring ribosomes upon in vitro translation and in live *E. coli* spheroplasts. In these polysomes, the ribosomes are arranged in a staggered or pseudohelical configuration along the mRNA trace, with the transcript being sequestered on the inside and the polypeptide exit sites facing the cytosol. Modeling of the elongating nascent polypeptide chains using the experimentally determined relative orientations of ribosomes suggests that this arrangement maximizes the distance between nascent chains on adjacent ribosomes. Thus, the 3D organization of polysomes, along with the shielding of nascent chains by molecular chaperones, may serve to increase the efficiency of folding of newly synthesized polypeptides.

RESULTS

Formation of Polysomes In Vitro

In vitro translation of truncated mRNAs of firefly luciferase (Luc) lacking a stop codon resulted in translational stalling of nascent chains (Figure 1A). Polysomes and 70S monoribosomes were readily detected by sucrose gradient centrifugation of the *E. coli* lysate following translation of constructs comprising the first 197, 371, or 550 amino acids of Luc (Luc 197–550) (Figure 1B and data not shown), covering the size range of typical *E. coli* cytosolic proteins (Kerner et al., 2005). Addition of RNase A or puromycin to the lysate prior to centrifugation disrupted the polysome structure (Kiho and Rich, 1964), resulting in a decrease in the size of the polysomal fraction and an increase in the 70S monoribosome fraction, as shown for Luc 371 (Figure 1B).

To confirm the presence of nascent chains in polysomes, we analyzed lysate samples by size exclusion chromatography. Upon translation in the presence of [^{35}S]Met, radiolabeled Luc 371 nascent chains were detected in polysomal fractions 1–2 and in monosomal fractions 3–5 eluted from the gel filtration column (Figure 1C, upper panel). Nascent chains in polysomes cover a range of sizes, forming a characteristic smear of bands, including the nonhydrolyzed peptidyl-tRNA (p-tRNA) of the 371 amino acid full-length product as the largest species. Polysomes were disrupted and nascent chains released upon treatment with EDTA and RNase A (Figure 1C, middle panel). A substantial fraction of the released chains cofractionated with the ~800 kDa chaperonin GroEL in fractions 5–9 (data not shown), suggesting that they were in a nonnative state. To visually confirm the

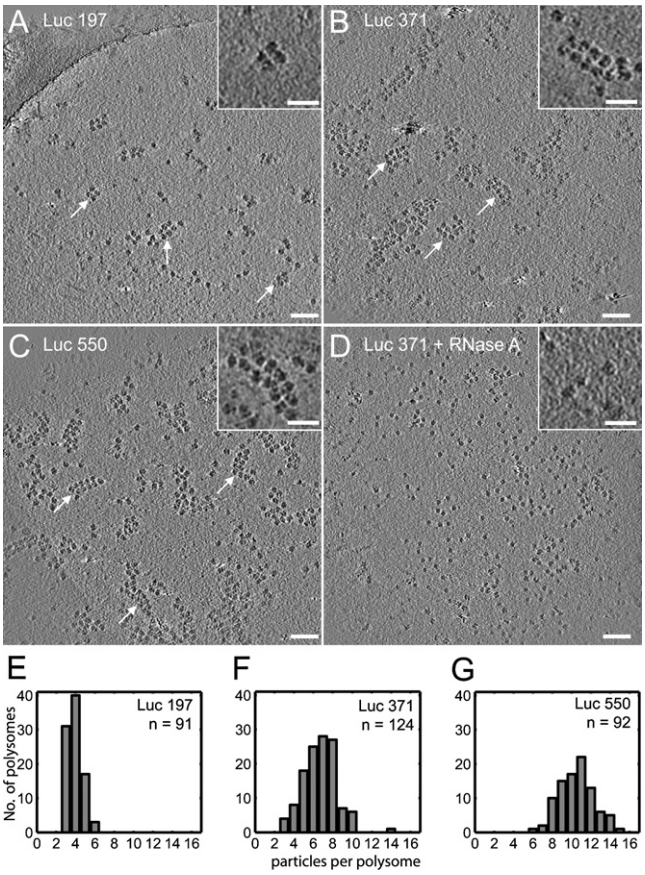

Figure 2. Polysomes in Tomograms of In Vitro Translation Reactions

(A–D) Slices of tomograms of vitrified *E. coli* lysates translating stalled Luc 197 (A), Luc 371 (B and D), and Luc 550 (C). The translation in (D) was treated with RNase A (scale bars, 100 nm). Polysomes are indicated by white arrows, with magnified, representative examples shown in inserts (scale bars, 50 nm).

(E-G) Distribution of the number of ribosomal particles per polysomal cluster for each Luc construct. n = number of polysomal clusters analyzed.

presence of polysomes versus monosomes, we subjected the respective peak fractions to CET (Figure 1D). As expected, fraction 2 contained predominantly polysomes (Figure 1D, left panel), whereas dispersed monosomes and some di- and trisomes were observed in reconstructed tomograms of fraction 4 (Figure 1D, right panel). Taken together, these results indicate the presence of ribosome-bound nascent chains in polysomes formed during in vitro translation. We chose to use nonfractionated samples for the following structural analysis to ensure the integrity of polysomes.

Observation of Large Polysomes Using CET

Nonfractionated translation lysate was diluted and vitrified for CET. In tomograms of lysates translating the truncated chains Luc 197, 371, and 550, ribosomal particles were observed in variable but distinct "double-row" arrays (Figures 2A–2C). In lysates translating full-length Luc mRNA and containing a stop codon, similar ribosome arrangements were seen but with a somewhat higher variability in overall shape (Figure S1A available online). This is expected because lysates translating the full-length protein contain a mixture of ribosomes at different stages of translation or (re)initiation, in contrast to lysates accumulating stalled nascent chains. For the truncated Luc 371 and Luc 550 transcripts, the majority of double-row polysome arrays lay roughly perpendicular to the tomographic z axis (electron-beam direction) (Figure 2B and C). Examples of smaller polysomes (Luc 197, 371) were oriented vertically in the ice layer. Additionally, we observed accumulations of ribosomes in tomograms that could not be visually distinguished from randomly clustered monosomes. However, the characteristic double-row species were exclusively found in translating lysate and were absent in RNase-A-treated (Figure 2D) and nontranslating control reactions (data not shown). Translation of nascent chains of the *E. coli* cytosolic protein galactitol-1-phosphate dehydrogenase (GatD) resulted in similar dense polysome arrangements, indicating that polysome formation is independent of the specific transcript used (Figure S1B).

In order to quantify the number of ribosomes per polysome array, we analyzed polysome complexes in tomograms and in 2D single projections in which ordered ribosome arrangements were clearly recognizable. For Luc 197, 371, and 550, the average numbers of ribosomes within putative polysomes were 4 ± 1, 8 ± 2, and 11 ± 2, respectively (Figures 2E–2G). Only ribosomal clusters in the characteristic arrangement were included in this analysis, whereas more unspecific clusters were not taken into account. Small polysomal arrangements (tri- or tetrasomes), formed by Luc 197, could only be recognized at higher sample dilutions.

Before further analyzing the spatial orientations of ribosomes within polysomes, we investigated whether similar polysome arrangements are found in lysates of actively growing *E. coli* cells, with and without heterologous protein expression. To this end, we expressed the model proteins Luc and Luc-SecM-GFP from arabinose-inducible plasmids. Luc-SecM-GFP is a fusion protein in which full-length luciferase is joined with green fluorescent protein (GFP) by the 17 amino acid stalling sequence of the SecM protein (Figure 3A). This sequence resulted in the synthesis of stalled nascent chains, as indicated by the production of truncated protein corresponding to full-length Luc in size and a range of shorter chains reactive with anti-Luc antibody (Figure 3B). Overexpression of similar constructs has been shown to result in the occupancy of a large fraction (~50%) of ribosomes with stalled nascent chains (Evans et al., 2005b). Polysomes were detected on density gradients with both stalled and nonstalled Luc constructs and also in control cells (Figure S2). CET of vitrified lysates from spheroplasts expressing Luc-SecM-GFP revealed large and highly ordered polysomes that corresponded closely to those found upon translation of stalled chains in vitro (Figure 3C, + ara). Polysome clusters with densely packed ribosomes were also observed in uninduced cells (Figure 3C, no ara), but these polysomes were generally smaller and less well defined in overall shape, as expected based on the smaller average size of endogenous *E. coli* cytosolic proteins (~300 aa) (Kerner et al., 2005). Accordingly, expression of nonstalled, full-length Luc (550 aa) resulted in the formation of some large, densely packed polysomes (Figure 3D, + ara). Thus, the polysomal arrangement in live *E. coli* cells is similar to that observed upon translation in vitro.

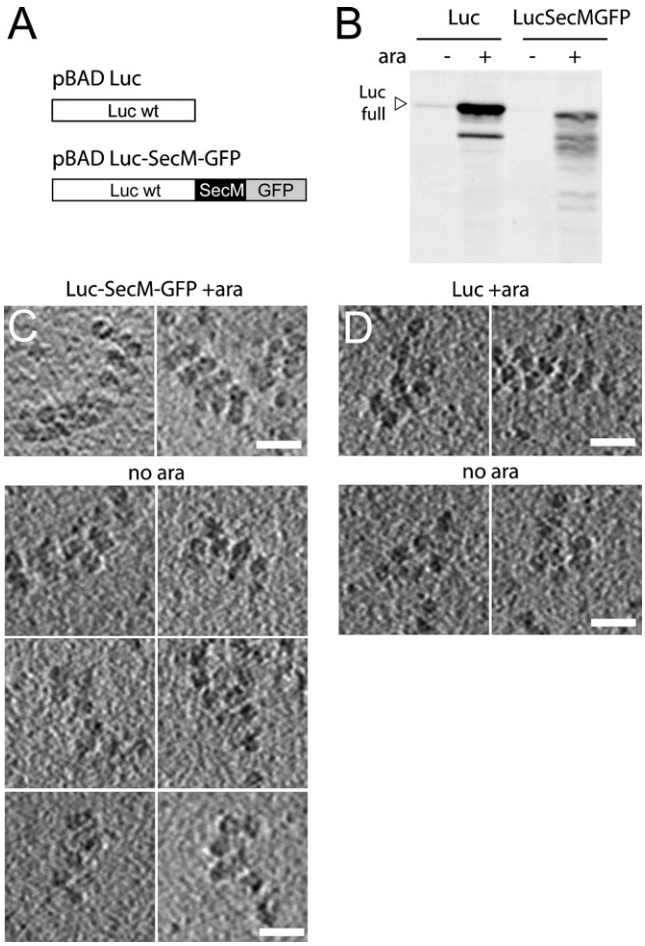

Figure 3. Polysomes in Tomograms of *E. coli* Spheroplast Lysates

(A) Schematic of the arabinose inducible model constructs *pBAD* Luc and *pBAD* Luc-SecM-GFP.

(B) Anti-Luc western blot showing in vivo expression of Luc and Luc-SecM-GFP proteins. Spheroplast lysate of uninduced (lanes 1 and 3) or arabinose-induced cells (lanes 2 and 4) was prepared after 30 min of incubation of cells with arabinose at 30°C.

(C) Subtomograms of spheroplast lysates from *E. coli* cells harvested 30 min after inducing Luc-SecM-GFP with arabinose (+ ara) or from uninduced control cells (no ara). Scale bars, 50 nm.

(D) Subtomograms of spheroplast lysates from *E. coli* cells harvested 120 min after inducing Luc (+ ara) or from control cells (no ara). Scale bars, 50 nm.

3D Organization of Polysomes

The spatial orientation of ribosomes in polysomes was determined by 3D template matching with a resolution-adjusted density derived from a 70S ribosome reference structure (Schuwirth et al., 2005). Particle coordinates and orientations in relation to the reference (Figure S3) were extracted from peaks in the resulting 3D crosscorrelation function (see Experimental Procedures).

The center-to-center distances between all ribosomes in individual tomograms from in vitro translations were calculated, allowing us to identify the closest neighbor(s) for each particle. With stalled polysomes, the 3D distribution of center-to-center distance vectors was clearly anisotropic, with a normal mean distance of 23 ± 2 nm (Figure S4). To test whether it was the polysomal species that exhibited this preferential relative positioning, we reconstructed and analyzed subvolumes containing polysomal arrangements from tomograms of lysates translating Luc 197, 371, and 550. Distance vectors from the center of mass of each identified polysomal ribosome to the center of mass of its closest neighbor particle clearly indicated preferential positioning at a distance around 22 ± 2 nm (Figures 4A–4C). By K-means minimization, two highly populated clusters of next neighbor center-to-center distance vectors were characterized that together represented 76% of the polysomal particles (Figures 4B and 4C). In relation to the reference ribosome orientation, a first cluster of distance vectors was found close to the mRNA entry site of each ribosome, and a second cluster was observed in the vicinity of the mRNA exit. We interpreted this clustering as preferential localization of neighbors around each polysomal particle *i* (Figure 1A), with the first neighboring ribosome located toward the 3′ end (*i-1* particle) and the second toward the 5′ end of the mRNA (*i+1* particle). Analysis of polysomes from spheroplasts showed similar but somewhat more variable center-to-center distance vectors of 24 ± 4 nm for nonstalled and 22 ± 3 nm for stalled ribosomes (Figure S5). Thus, the 3D organization of polysomes in vivo, while somewhat less compact, shares the principal organization of the dense polysomes formed in vitro.

To further define the preferential orientations of adjacent ribosomes in polysomes, we expanded the classification of polysomal particles generated in vitro to a set of 2393 ribosomes from 12 tomograms. Three distance vectors were calculated between the center of mass of ribosomes *i* and three points in the neighboring particles. For a class of ~600 particles that had a neighbor near the *i+1* centroid, all three vectors clustered to distinct positions, revealing at least two subclasses of adjacent particle orientations (Figure 4D). In both subclasses of *i+1* neighbors, 90% of the 30S ribosomal subunits face the 30S of particle *i*, but their orientations differ in an ~180° rotation about the y axis of the chosen coordinate system. We designated these subsets of orientation classes as "top-to-top" (t-t) and "top-to-bottom" (t-b) (Figure 4D). The average distance between the mRNA exit *i* and the mRNA entry *i+1* was about 5.5 nm (σ_{std} = 1.1 nm) in both classes, indicating the presence of a small gap between the 30S subunits.

Relative orientations between each ribosome *i* and any adjacent neighbor *k* were also described as a set of three angles $(\varphi, \theta, \psi)_{ik}$. The relative angular distribution again displays a preferential orientation between neighboring ribosomal particles. Ribosomes having a neighbor at the *i+1* centroid display at least two characteristic clusters of relative orientations, corresponding to the t-t or t-b arrangement, respectively. At least two clusters of relative orientations were also found for the *i-1* neighbors (Figure S6).

Having confirmed that neighboring ribosomes in polysomes adopt preferred orientations, the averages of classified subtomograms, each containing a polysomal particle and its surrounding, were expected to show clear densities of polysomal neighbors. Applying the initial orientations found by template matching, these subvolumes were 3D aligned and averaged to produce an initial density map. During further iterative alignment

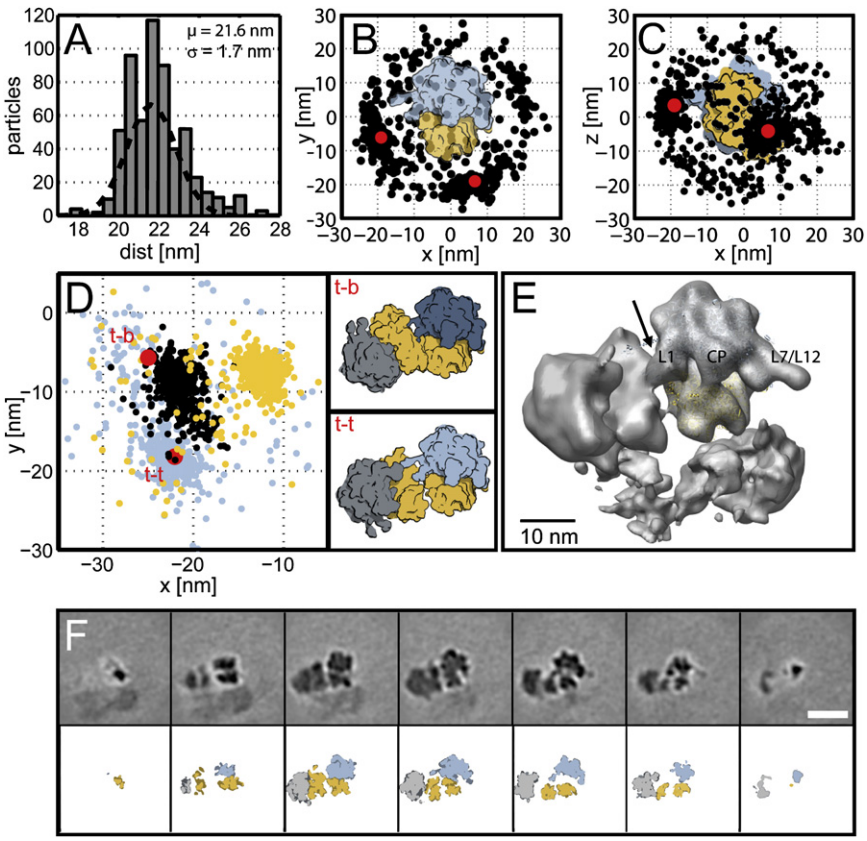

Figure 4. Spatial Relationship of Polysomal Ribosomes

(A) Distribution of distances of a set of ribosomal particles to their next neighbor ribosome in polysomes formed in vitro with Luc 197, Luc 371, and Luc 550. Gaussian fitting (dashed line) indicates a mean center-to-center of mass distance of 21.6 nm.

(B and C) 3D distance vectors in polysomes. An x,y plot (B) and an x,z plot (C) showing the distribution of center-to-center 3D distance vectors (black dots) from each ribosome to its next neighbor. Two major K-means clusters (gray dots at (x,y,z) = 6.7 nm, −18.3 nm, −2.9 nm, and at x,y,z = −18.6 nm, −5.5 nm, 0.8 nm) were observed relative to the ribosomal reference structure.

(D) x,y plot of the 3D distance vectors from classified particles to their *i+1* neighbor from center of mass to either center of mass (black dots) or to the mRNA entry site (yellow dots) or to a point close to protein L9 in the large ribosomal subunit (light blue dots). K-means calculations revealed two clusters of vectors (red dots) that represent two orientation classes named t-b and t-t. The two orientation classes are depicted in the subpanels.

(E) Putative contact sites between adjacent ribosomes in polysomes (arrows) as seen in the averaged 3D density of class t-t ribosomes. The reference crystal structure was docked into the experimental density with the 50S and 30S subunits in blue and yellow, respectively.

(F) Single z slices (increments of 3.4 nm) of the density map of averaged particles as in Figure 4E. Scale bar, 25 nm.

with decreasing angle increments, a spherical mask was chosen to exclude any surrounding densities of each particle. In an initial average of all polysomal particles having neighbors either at the *i+1*, *i-1*, or both positions, two large additional densities were found outside of the alignment mask. Further classification of 595 particles with an *i+1* neighbor was performed according to the relative orientation criteria, as described above. In an average of 391 particles in the t-t orientation (Figures 4E and 4F), the central particle resembles the 70S ribosome structure at a resolution of about 3 nm, at which distinct features can be resolved. Most notably, a large additional density, attributable to the *i+1* neighbor and not involved in the alignment, appears near the mRNA exit of this class average, with the shape and orientation of the adjacent ribosome recognizable at low resolution (Figures 4E and 4F).

In the t-t average, the 30S subunits of the central particle *i* and the *i+1* neighbor are facing each other, bringing the mRNA exit of the central particle into the vicinity of the entry of its *i+1* neighbor. A continuous density between the L1 stalk of ribosome *i* and the 30S subunit of the *i+1* ribosome could be detected (Figure 4E), possibly reflecting a connectivity between adjacent ribosomes. In order to estimate the position of the connecting density in the t-t class of polysomal ribosomes, two copies of the reference ribosome structure were docked into the class average map. Although the accuracy of the docking at position *i+1* is limited, the docked atomic coordinates suggest that the connecting density extends from the L1 arm of ribosome *i* to a region in the 16S rRNA (U407–A434) or protein S4 of the *i+1* ribosome. The L1 stalk is known to adopt different positions in the translational cycle (Valle et al., 2003b). Thus, the functional significance of this connectivity, if any, remains to be determined. Smaller, more flexible or substoichiometric ribosome-bound components, including the chaperone trigger factor, the L12 stalk of the ribosome, and translation factors could not be seen in the averaged structure. Likewise, the additional density of the mRNA could not be unambiguously assigned. For the average of ribosomes in the t-b class (116 particles), only a very diffuse density of either the *i+1* or the *i-1* neighbor particle was averaged (data not shown), reflecting a higher variance in orientation within this class.

Models of Polysomes

To better understand the common elements in polysomal organizations, we generated 3D models for a large set of polysomes observed in tomograms (Figures 5 and S7 and Movies S1 and S2). In each case shown, the observed topologies can be understood by viewing the two neighboring particle classes (t-t and t-b) described as building blocks above. The t-t configuration was found more frequently (Figure 4D), and, in rare cases, all particles throughout a polysome exclusively adopted the t-t configuration, resulting in a highly characteristic pseudohelical arrangement (Figure 5A). A well-defined pseudoplanar arrangement

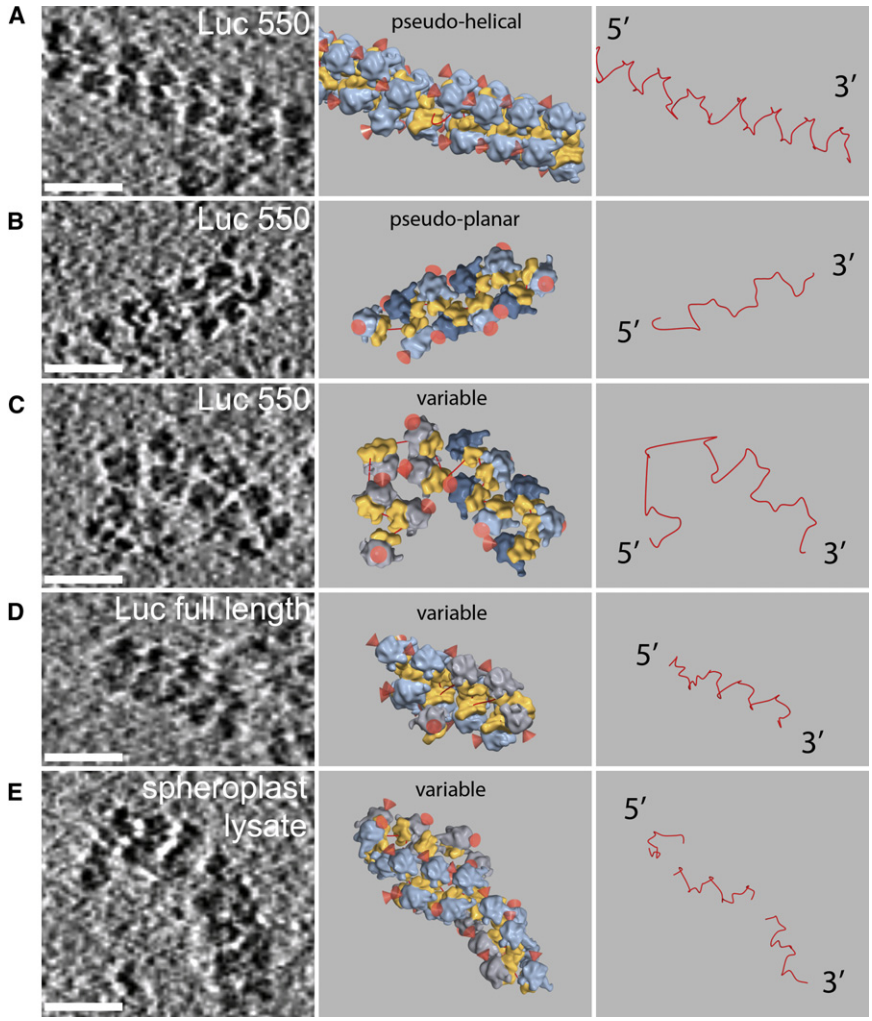

Figure 5. Polysomes Have Characteristic Topologies

(A–E, left) Tomographic slices of three classes of polysome organizations. Examples from in vitro translation of stalled Luc 550 (A–C), nonstalled full-length Luc (D), and in vivo expression in spheroplasts induced to express Luc-SecM-GFP (E) are shown (scale bars, 50 nm). See Figure S7 for additional examples.

(A–E, middle) Isosurface representations of single ribosomes (large subunit, blue; small subunit, yellow) were placed into corresponding experimental positions (light blue, t-t; dark blue, t-b). Red cones point to the peptide exit tunnel on each 50S subunit. Dark gray representation was inserted for ribosomes not unambiguously assigned to the polysome. The organization classes are indicated above each model.

(A–E, right) The putative mRNA pathway with the shortest distance between each ribosome is shown in red. In (A), the trace shows a helical pathway and in (B), a roughly "sinusoidal" pathway, as compared to the more variable arrangements.

composed of alternating t-t and t-b configurations is shown in Figure 5B. In the majority of polysomes, however, next-neighbor configurations were more varied, and, hence, a less defined organization was observed, especially toward the 5′ end (Figures 5C–5E). We found small segments of pseudohelical polysome organization with the longitudinal axes both in the ice plane and perpendicular to it (Figure S7A). Thus, any effects of ice thickness or interactions with the air-ice surface appear not to impose a particular polysome organization.

For the purpose of visualization, the putative mRNA pathway was drawn between mRNA exit and entry sites in neighboring ribosomes (Figure 5, right panels); the obvious nature of this pathway allowed us to unambiguously assign the sequence of ribosomes along the mRNA in the 3′ to the 5′ direction (see below). Interestingly, in all cases where the ribosomes are densely packed (Figures 5A, 5B, 5D, 5E, and S7), the putative mRNA trace is sequestered on the inside while both the polypeptide exit sites and the tRNA entrance sites remain accessible from the outside. We also examined several stalled polysomes from spheroplasts. A representative example in a variable organization is shown in Figure 5E and is very similar to variable polysome arrangements generated in vitro (Figures 5C and 5D). Due to their higher variability, putative mRNA traces of nonstalled polysomes in vivo could only be delineated for shorter polysome segments of three to four consecutive ribosomes (within the context of larger polysomes) but notably displayed the same principal configuration between ribosome pairs seen in larger polysomes in vitro (data not shown).

The distance between codon recognition sites in densely packed neighboring ribosomes was estimated as follows. Positions of 26 nucleotides resolved in a 70S ribosomal crystal structure containing mRNA (Yusupova et al., 2006) were used in the polysomal model for each ribosome. Between two adjacent ribosomes, an average distance of 7 ± 1 nm was determined from the exit site of the mRNA of one ribosome to the entrance site of the next ribosome. With a worm-like chain model (Supplemental Experimental Procedures), we estimated an additional number of 46 ± 6 nucleotides bridging adjacent mRNA exit and entry points, giving, on average, a total of up to 72 nucleotides between codon recognition sites. This would correspond to a difference in length of 24 residues of nascent peptides between neighboring ribosomes.

To gain insight into the potential proximity of nascent peptides in the context of polysomes, we determined the pairwise distances between the peptide tunnels of adjacent ribosomes. The average distance for the sites of peptide exit at a position close to ribosomal protein L23 in each particle *i* and its next neighbor was 29 ± 1 nm. A visual inspection of the modeled polysomes with pointers at the peptide tunnels (Figure 5, middle panels) indicated that the closest peptide exit site is not found on the *i+1* or *i-1* but on the *i*+3 ribosome, with an average

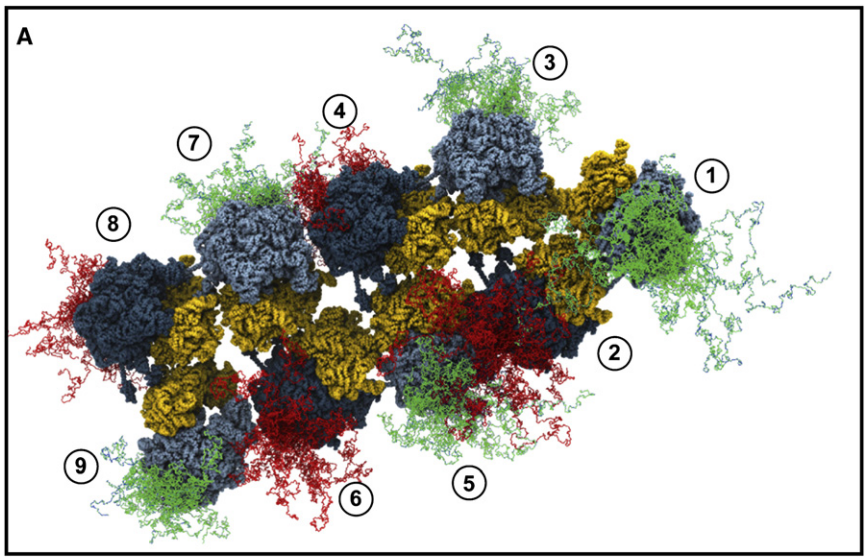

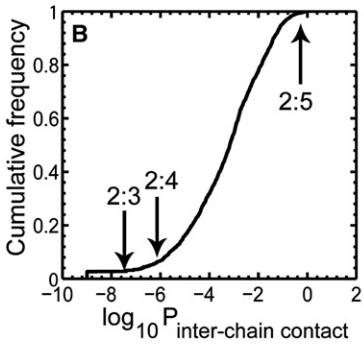

Figure 6. Models of Nascent Chain Configurations in a Representative Polysome

(A) Twenty nascent chain conformations were built at each ribosome position in the pseudoplanar polysome shown in Figure 5B. Chains at odd-numbered ribosomes are colored green, and chains at even-numbered ribosomes are red. The length of each nascent chain is estimated as described in Results and Supplemental Experimental Procedures.

(B) Cumulative histogram of the probability of interchain contacts between modeled nascent chains populating unfolded, compact conformations in 1500 randomly rotated but physically adjacent ribosome pairs. Arrows mark the probability of forming interchain contacts in the ribosome orientations that are actually observed in the polysome (Figure 5B and Supplemental Experimental Procedures).

distance of ~15 nm. This was most evident in highly ordered polysome arrangements (Figures 5A and 5B).

Conformational Modeling of Nascent Chains in Polysomes

Interactions between nascent polypeptide chains in polysomes have been implicated as a cause of protein misfolding and aggregation, based on the view that nascent chains populate unfolded states, at least until complete folding units (domains) have emerged from the ribosome (Hartl and Hayer-Hartl, 2002). To estimate the potential for such interactions, we employed pseudoatomic models of ribosomes in an experimentally determined pseudoplanar polysome organization (Figure 5B). This polysome array displays a range of neighbor-neighbor configurations and is representative of the relative ribosome orientations in different polysome structures described. For each of the ribosomes in the pseudoplanar polysome, we modeled thousands of putative nascent chain conformers with dimensions consistent with unfolded but compact random coils in the absence of molecular chaperones, thus maximizing possible nascent chain interactions (Figure 6A and Supplemental Experimental Procedures). The probabilities of interchain contacts found in this arrangement were then compared to those in control simulations with 1500 randomized ribosome orientations. Strikingly, ribosome pairs 2:3 and 2:4 of the polysome complex exhibited nascent chain contact probabilities that were comparable with the very lowest found among the 1500 randomized orientations, whereas the ribosome pair 2:5 showed a contact probability similar to the highest value found in any of the randomized orientations (Figure 6B, arrows). Based on these simulations, it appears that the experimentally determined ribosome orientation in polysomes serves to minimize the probability of contacts between nascent chains on ribosomes that are consecutively arranged on the mRNA. The shielding of nascent chains by molecular chaperones, such as trigger factor, would further reduce the probability of intrapolysomal chain aggregation.

DISCUSSION

Dense Packing of Ribosomes in Polysomes

Employing cryoelectron tomography and template matching, we have described the 3D supramolecular organization of native bacterial polysomes. Our analysis reveals a remarkably well-defined arrangement of ribosomes in staggered or helical orientations, with the mRNA being sequestered on the inside, while the tRNA entrance sites and the polypeptide exit sites are exposed to the cytosol. While particularly large and densely packed polysomes are most prominent upon translational stalling, polysomes displaying very similar or identical orientations are also observed in vitrified lysates of actively translating *E. coli* cells.

Our results indicate that a tightly packed arrangement of ribosomes during protein synthesis in the context of polysomes is physiologically meaningful. These arrangements are generally observed between neighboring ribosomes independent of polysome size but seem to be particularly favored under conditions in which the rate of translation initiation exceeds that of elongation

or termination. Initiation is thought to be the rate-limiting step in determining polysome density in vivo and in vitro (Antoun et al., 2006; Spirin, 2004). Alternatively, when the supply of translation cofactors, energy, and aminoacyl-tRNA diminishes or clusters of rare codons are encountered, elongation speed (normally $\sim$20 aa s^{-1}) becomes rate limiting, resulting in ribosomal pausing or stalling. Indeed, transient ribosome pausing at rare codons with correspondingly rare tRNAs is considered a relatively frequent occurrence serving various physiological functions (Buchan and Stansfield, 2007). It may be employed as a regulatory mechanism known as transcriptional attenuation, as in the case of the *E. coli trp* operon, or may serve to assist the folding of nascent polypeptides at the level of domains (Evans et al., 2005a). A high degree of ribosomal occupancy of the mRNA is known to be protective against endonucleolytic cleavage (Arnold et al., 1998). The polysomal models that we report here raise the intriguing possibility that this protection may not simply be a product of the ribosomes directly covering the mRNA but may also be a result of the sequestering of the RNA within the higher-order supramolecular polysome assembly.

Ribosomal Architecture as a Determinant for Polysomal Organization

A notable characteristic of the polysomal arrangements described in this study is the clear preferential 3D orientation between adjacent ribosomes. We observed a defined "inward" positioning of the 30S ribosomal subunit and an "outward" or "cytosolic" orientation of the 50S subunit. At least two configurations of neighbor orientations are possible and were generally observed in stalled and actively translating polysomes. The t-b configuration has a broader angular distribution and occurs in pseudoplanar polysomes in a 1:1 ratio relative to the t-t configuration. The t-t configuration exhibits a more defined relative orientation and, when predominant, leads to a helical or solenoid arrangement of polysomes. Its class average resembles the orientation of two *E. coli* ribosomes found in the crystal unit cell (Schuwirth et al., 2005). Interestingly, an additional density, presumably involving the L1 stalk region, appears to bridge the gap between two ribosomal neighbors in polysomes. This contact may induce a preferential orientation of polysomal neighbors.

Two patterns of mRNA traces are most plausible in our polysome models: a sinusoidal path in pseudoplanar polysomes and a pseudohelical path in helical polysomes. Some earlier observations of negatively stained polysomes also suggested a helical mRNA path (Slayter et al., 1968), whereas other studies described irregular distances between ribosomes (Friedberg et al., 1975). The mRNA conformation is expected to be more constrained at a higher density of ribosome packing, and the well defined organization reported here is probably close to the densest possible arrangement.

It will be interesting to compare the 3D topologies of prokaryotic and eukaryotic polysomes. In eukaryotes, a pseudocircularization of the mRNA has been proposed for active polysomes in yeast (Tarun and Sachs, 1996; Wells et al., 1998), mammals (Craig et al., 1998), and wheat germ lysate (Kopeina et al., 2008; Madin et al., 2004). However, a tomographic analysis is not yet available for any of these systems. While it would be desirable to unambiguously recognize active ribosomes in tomograms in an intact cellular environment (Ortiz et al., 2006), the classification of tomographic particle reconstructions from such specimens remains a challenging task (Forster et al., 2008). In the case of polysomes in lysates, we applied a supervised classification by taking advantage of preferential orientations between adjacent polysomal ribosomes. In future studies, this criterion should facilitate the recognition of translating ribosomes in a cellular context and allow the correlation of their spatial distribution with other large complexes involved in protein processing.

Implications for Protein Synthesis

It is generally thought that the ribosomal exit tunnel provides very limited space for the folding of the elongating polypeptide chain, allowing only for the formation of α-helical elements. Most secondary structure and essentially all tertiary interactions must form during co- or posttranslational folding (Hartl and Hayer-Hartl, 2002; Lu and Deutsch, 2005; Woolhead et al., 2004). In the model proteins examined here, the nascent chain is shielded from the cytosol by the ribosome-associated chaperone trigger factor (Kaiser et al., 2006; Tomic et al., 2006), and its folding is assisted by the Hsp70 chaperone system (DnaK/DnaJ/GrpE) (Agashe et al., 2004). Double deletion of TF and DnaK (Hsp70) leads to severe protein aggregation and is lethal in *E. coli* at growth temperatures above 30°C (Deuerling et al., 1999; Teter et al., 1999). In the absence of sufficient protection by chaperones, folding intermediates tend to aggregate in the highly crowded cellular environment.

Aggregation may initiate in the context of polysomes where identical unfolded polypeptides reach high local concentrations, but little evidence in support of this frequently stated proposition is available. Based on our structural analysis and the simulation of the conformational space of nascent chains, we suggest that the specific 3D organization of polysomes serves to deter nascent chain interactions between ribosomes that are consecutively arranged along the mRNA. Interchain contacts may, however, occur from the *i* to the *i+3* neighboring ribosome, particularly when assuming unfolded chain conformations. Notably, in the polysome structures analyzed, the *i* and *i+3* nascent chains would differ by $\sim$72 amino acids in length, equivalent to a small folding domain (compare ribosomes 2:5 in Figure 6A). Thus, the *i* nascent chain may be capable of significant compaction, which would reduce the exposure of hydrophobic residues and the propensity for coaggregation. In light of our findings, it appears possible that the main function of chaperones that interact with nascent polypeptides is not to suppress nascent chain aggregation within polysomes but, rather, to reduce intrachain misfolding as well as aggregation between different polysomes in the crowded cellular environment. The supramolecular arrangement of polysomes and the chaperone machinery may have coevolved to ensure efficient de novo protein folding.

EXPERIMENTAL PROCEDURES

Template Preparation and Cell-Free Protein Synthesis

Luc-SecM-GFP was cloned into a *pBAD33* vector and encodes full-length Luc followed by the linker IEGRGSGTS, the 17 amino acid SecM stalling sequence

FSTPVWISQAQGIRAGP, the linker AAIG, and GFP lacking the two N-terminal amino acids. *pBAD* Luc (Agashe et al., 2004), *pET15b*, and the primers to generate PCR products as templates for in vitro transcription were as described previously (Tomic et al., 2006). Primer 5′-GGATCCTCGAGG ATCCTTATTAC-3′ was used for full-length constructs. Luc mRNA was transcribed in vitro from PCR templates (Ambion) and purified (QIAGEN). In vitro translation reactions were performed in an *E. coli*-derived translation lysate (Roche) as previously described (Agashe et al., 2004), except that reactions contained 0.2 μCi/μl [^{35}S]Met and 250 nM mRNA. Translation was stopped by incubation on ice for 10 min with 200 ng/μl chloramphenicol (Cam).

Translation reactions were directly analyzed on SDS-PAGE or following size exclusion chromatography on a Superose 6 column in buffer containing 20 mM HEPES (pH 7.5), 100 mM KOAc, 14 mM $Mg(OAc)_2$, and 2 mM β-mercaptoethanol. To disrupt 70S particles and tRNA, we incubated reactions with 0.2 μg/ml RNase A and 10 mM EDTA for 10 min at 30°C.

Polysome Preparation from *E. coli* Spheroplasts

Luc and Luc-SecM-GFP were expressed in *E. coli* MC4100 by induction with 0.5% arabinose for 30 min at 30°C. The cells were rapidly chilled on ice, harvested by short centrifugation, and resuspended in 50 mM Tris-Cl (pH 8.0), 0.5 M sucrose, and 100 μg/ml Cam. Lysozyme (Sigma) was added at a concentration of 0.8 mg/ml for 5 min at 4°C, followed by incubation with 2.5 mM EDTA for 5 min at 4°C. The reaction was diluted in 50 mM Tris-Cl (pH 8.0) and incubated for 5 min at 30°C before the addition of an equal volume of lysis buffer (50 mM Tris-Cl (pH 7.5), 5 mM $MgSO_4$, 0.2% Triton X-100, 5 U/ml DNase I, and 100 μg/ml Cam). After incubation for 10 min on ice, cell debris was removed by centrifugation at 20.000 × g before analyzing the lysate by SDS-PAGE or density gradient centrifugation.

Density Gradient Centrifugation

In vitro translation reactions were separated on 10%–40% (w/v) sucrose density gradients prepared in 20 mM Tris-Cl (pH 7.5), 10 mM $MgCl_2$, 100 mM NH_4Cl, and 2 mM DTT. A 50 μl reaction was layered over the gradient and centrifuged for 90 min at 160,000 × g (Beckman SW 41 Ti) at 4°C. Control translations were treated with 0.1 μg/ml RNase A for 1 min at 25°C. Elution and fractionation were done top to bottom, and chromatograms were recorded at 254 nm.

Cryoelectron Tomography

In vitro translation reactions were diluted 2.5- to 3.5-fold in 20 mM Tris-Cl (pH 7.5) and 10 mM $MgCl_2$. Colloidal gold markers (8 nm) were applied to 400 mesh holey carbon grids (Quantifoil, Germany). The diluted samples (3 μl) were added, incubated for 30 s, blotted with filter paper for 3–5 s, and vitrified in liquid ethane at −196°C. CETs were recorded on a CM 20 FEG instrument (Philips, Eindhoven, Netherlands) run at 160 kV acceleration voltage and a nominal underfocus of Δz = 3 μm. Single-axis tilt series were recorded between −60° and +60° with a tilt angle increment of 3° and with the cumulative electron dose not exceeding 50 $e^-/Å^2$. Data acquisition was carried out using a 4096 × 4096 slow-scan CCD camera and control software for automated image tracking and focusing (TVIPS, Germany). The micrographs were visually aligned by tracking the ice-embedded gold markers. The 3D reconstructions were performed by weighted backprojection implemented in the TOM software package (Nickell et al., 2005).

Template Matching and Classification

Overview tomograms at a high binning factor ([2.24 nm]^3/voxel) or lower-binned subtomograms ([1.12 nm]^3/voxel) of selected regions were reconstructed. Probing of these tomographic volumes with a 3D template structure was done as described (Frangakis et al., 2002). The template structure was generated from the atomic models of the *E. coli* ribosome 3.5 Å crystal structure (PDB entries 2AW7 and 2AWB) (Schuwirth et al., 2005), rotated (Figure S3), adjusted to the corresponding voxel size of the reconstructed volumes, and bandpass filtered to a resolution of 4 nm. The crosscorrelation function was calculated in parallel for 10° incremental steps of Euler angles and coordinates in Fourier space. Locally normalized peaks of CCCs were found wherever the missing-wedge-corrected reference structure correlates best with the experimental densities during scanning of the tomogram in three translational and rotational dimensions. The highest CC peaks with a predefined minimum radius were extracted, yielding the corresponding 3D coordinates for each particle *i* (x_i, y_i, and z_i) and Euler angles (φ_i, θ_i, and ψ_i) in relation to the reference (Figure S3). Subvolumes of selected particles were reconstructed with a voxel size of (0.56 nm)^3 and subjected to further classification, alignment, and averaging. The resolution of the average ribosome map was determined by Fourier shell correlation of two averages, each derived from half of the collected particles using a coefficient of 0.5 as a threshold. Models for polysomal topologies can be reduced to the characterization of just two neighboring particles as elemental unit of polysomes; the relative orientations between a polysomal particle *i* and its two next neighbors *k (= i+1* or *i-1)* are, in principle, redundant. To describe the organization, it proved useful to calculate a set of three distance vectors from the center of each particle to three defined points of its next neighbor. Distance vectors were calculated from the center of ribosome *i* to three different positions in the neighbor ribosome k: the center of mass of *k*, a position near the 30S neck of *k* (x, y, z = 1.1 nm, −9.5 nm, −0.6 nm), and a position near protein L9 of *k* (x, y, z = 12.2 nm, 0.6 nm, 1.1 nm). These vectors were rotated using the corresponding orientations determined for each ribosome *i* to reorient them with respect to a common reference. For classification of particles sharing a similar arrangement to a neighbor, 3D clustering by K-means was used in two subsequent steps: the first, only considering center-to-center vectors (neighbors at similar location) and the second, using the center-to-L9 vectors (neighbors with a similar orientation). Clustering was not qualitatively affected, varying the start seed selection (sampled or random).

Polysome and mRNA Modeling

To visualize the 3D arrangement of reconstructed polysomes, original ribosomal densities in tomograms were substituted by the masked and filtered 70S ribosome isosurface derived from the average of polysomal ribosomes. This average was positioned with the original coordinates and orientations of identified polysomal particles. To model a probable mRNA pathway throughout polysomal arrangements, three points in each ribosome *i* were defined corresponding to the mRNA entry $(x,y,z)_i$ = (1.1, −9.5, −0.6), the mRNA exit $(x,y,z)_i$ = (−1.7 nm, 8.3 nm, −3.3 nm), and the codon recognition site $(x,y,z)_i$ = (0 nm, −5 nm, 3.4 nm). These anchor coordinates on the expected mRNA path were chosen according to the positions found for 5′ or 3′ nucleotides in the crystal structure of the *T. thermophilus* ribosome containing mRNA (PDB entry 2HGR) (Yusupova et al., 2006). The putative mRNA path was drawn as a flexible rod joining the three coordinates in each ribosome *i* and linking its mRNA exit with the closest positioned mRNA entry of the next 5′ *(i+1)* neighbor. A physically more meaningful estimate of nucleotides between adjacent codon recognition sites was derived from a worm-like chain with 26 nucleotides inside each ribosome (Yusupova et al., 2006) with an assumed persistence length of 0.79 nm for single-stranded RNA in ribosome-mRNA complexes (Vanzi et al., 2005).

Construction of Putative Nascent Chain Conformations

Putative nascent chain conformations were modeled with a simplified (C_α only) model of protein structure. The procedure of structural modeling of both the nascent chains and the ribosomes was as described recently (Elcock, 2006) (see Supplemental Experimental Procedures).

ACCESSION NUMBERS

The cryo-EM map of the *E. coli* class t-t ribosomes was deposited in the Electron Microscopy Data Bank under accession code EMD-1582.

SUPPLEMENTAL DATA

The Supplemental Data include Supplemental Experimental Procedures, seven figures, and two movies and can be found with this article online at http://www.cell.com/supplemental/S0092-8674(08)01491-8.

ACKNOWLEDGMENTS

We thank S.K. Lakshmipathy for providing the *pBAD* Luc-SecM-GFP construct. This work was supported by Framework 7 Program of the European

Union, by "Fondation Fourmentin Guilbert," and by the Deutsche Forschungsgemeinschaft (FOR 967).

Received: July 24, 2008
Revised: October 12, 2008
Accepted: November 13, 2008
Published: January 22, 2009

REFERENCES

Agashe, V.R., Guha, S., Chang, H.C., Genevaux, P., Hayer-Hartl, M., Stemp, M., Georgopoulos, C., Hartl, F.U., and Barral, J.M. (2004). Function of trigger factor and DnaK in multidomain protein folding: Increase in yield at the expense of folding speed. Cell *117*, 199–209.

Agrawal, R.K., Spahn, C.M., Penczek, P., Grassucci, R.A., Nierhaus, K.H., and Frank, J. (2000). Visualization of tRNA movements on the Escherichia coli 70S ribosome during the elongation cycle. J. Cell Biol. *150*, 447–460.

Antoun, A., Pavlov, M.Y., Lovmar, M., and Ehrenberg, M. (2006). How initiation factors tune the rate of initiation of protein synthesis in bacteria. EMBO J. *25*, 2539–2550.

Arnold, T.E., Yu, J., and Belasco, J.G. (1998). mRNA stabilization by the ompA 5′ untranslated region: Two protective elements hinder distinct pathways for mRNA degradation. RNA *4*, 319–330.

Ban, N., Nissen, P., Hansen, J., Moore, P.B., and Steitz, T.A. (2000). The complete atomic structure of the large ribosomal subunit at 2.4 Å resolution. Science *289*, 905–920.

Baram, D., Pyetan, E., Sittner, A., Auerbach-Nevo, T., Bashan, A., and Yonath, A. (2005). Structure of trigger factor binding domain in biologically homologous complex with eubacterial ribosome reveals its chaperone action. Proc. Natl. Acad. Sci. USA *102*, 12017–12022.

Bashan, A., and Yonath, A. (2005). Ribosome crystallography: Catalysis and evolution of peptide-bond formation, nascent chain elongation and its co-translational folding. Biochem. Soc. Trans. *33*, 488–492.

Bohm, J., Frangakis, A.S., Hegerl, R., Nickell, S., Typke, D., and Baumeister, W. (2000). Toward detecting and identifying macromolecules in a cellular context: Template matching applied to electron tomograms. Proc. Natl. Acad. Sci. USA *97*, 14245–14250.

Buchan, J.R., and Stansfield, I. (2007). Halting a cellular production line: Responses to ribosomal pausing during translation. Biol. Cell *99*, 475–487.

Craig, A.W., Haghighat, A., Yu, A.T., and Sonenberg, N. (1998). Interaction of polyadenylate-binding protein with the eIF4G homologue PAIP enhances translation. Nature *392*, 520–523.

Deuerling, E., Schulze-Specking, A., Tomoyasu, T., Mogk, A., and Bukau, B. (1999). Trigger factor and DnaK cooperate in folding of newly synthesized proteins. Nature *400*, 693–696.

Elcock, A.H. (2006). Molecular simulations of cotranslational protein folding: Fragment stabilities, folding cooperativity, and trapping in the ribosome. PLoS Comput. Biol. *2*, e98.

Evans, M.S., Clarke, T.F., and Clark, P.L. (2005a). Conformations of co-translational folding intermediates. Protein Pept. Lett. *12*, 189–195.

Evans, M.S., Ugrinov, K.G., Frese, M.A., and Clark, P.L. (2005b). Homogeneous stalled ribosome nascent chain complexes produced in vivo or in vitro. Nat. Methods *2*, 757–762.

Forster, F., Pruggnaller, S., Seybert, A., and Frangakis, A.S. (2008). Classification of cryo-electron sub-tomograms using constrained correlation. J. Struct. Biol. *161*, 276–286.

Frangakis, A.S., Bohm, J., Forster, F., Nickell, S., Nicastro, D., Typke, D., Hegerl, R., and Baumeister, W. (2002). Identification of macromolecular complexes in cryoelectron tomograms of phantom cells. Proc. Natl. Acad. Sci. USA *99*, 14153–14158.

Friedberg, I., Herzberg, M., Zarivatch, S., and Ron, E.Z. (1975). Polysomes in Escherichia coli during amino acid starvation: Structural change observed by electron microscopy. FEBS Lett. *56*, 108–110.

Gabashvili, I.S., Agrawal, R.K., Spahn, C.M., Grassucci, R.A., Svergun, D.I., Frank, J., and Penczek, P. (2000). Solution structure of the E. coli 70S ribosome at 11.5 Å resolution. Cell *100*, 537–549.

Hartl, F.U., and Hayer-Hartl, M. (2002). Molecular chaperones in the cytosol: From nascent chain to folded protein. Science *295*, 1852–1858.

Hsu, S.T., Fucini, P., Cabrita, L.D., Launay, H., Dobson, C.M., and Christodoulou, J. (2007). Structure and dynamics of a ribosome-bound nascent chain by NMR spectroscopy. Proc. Natl. Acad. Sci. USA *104*, 16516–16521.

Kaiser, C.M., Chang, H.C., Agashe, V.R., Lakshmipathy, S.K., Etchells, S.A., Hayer-Hartl, M., Hartl, F.U., and Barral, J.M. (2006). Real-time observation of trigger factor function on translating ribosomes. Nature *444*, 455–460.

Kerner, M.J., Naylor, D.J., Ishihama, Y., Maier, T., Chang, H.C., Stines, A.P., Georgopoulos, C., Frishman, D., Hayer-Hartl, M., Mann, M., et al. (2005). Proteome-wide analysis of chaperonin-dependent protein folding in Escherichia coli. Cell *122*, 209–220.

Kiho, Y., and Rich, A. (1964). Induced enzyme formed on bacterial polyribosomes. Proc. Natl. Acad. Sci. USA *51*, 111–118.

Kopeina, G.S., Afonina, Z.A., Gromova, K.V., Shirokov, V.A., Vasiliev, V.D., and Spirin, A.S. (2008). Step-wise formation of eukaryotic double-row polyribosomes and circular translation of polysomal mRNA. Nucleic Acids Res. *36*, 2476–2488.

Lu, J., and Deutsch, C. (2005). Folding zones inside the ribosomal exit tunnel. Nat. Struct. Mol. Biol. *12*, 1123–1129.

Lucic, V., Forster, F., and Baumeister, W. (2005). Structural studies by electron tomography: From cells to molecules. Annu. Rev. Biochem. *74*, 833–865.

Madin, K., Sawasaki, T., Kamura, N., Takai, K., Ogasawara, T., Yazaki, K., Takei, T., Miura, K., and Endo, Y. (2004). Formation of circular polyribosomes in wheat germ cell-free protein synthesis system. FEBS Lett. *562*, 155–159.

Nickell, S., Forster, F., Linaroudis, A., Net, W.D., Beck, F., Hegerl, R., Baumeister, W., and Plitzko, J.M. (2005). TOM software toolbox: Acquisition and analysis for electron tomography. J. Struct. Biol. *149*, 227–234.

Ortiz, J.O., Forster, F., Kurner, J., Linaroudis, A.A., and Baumeister, W. (2006). Mapping 70S ribosomes in intact cells by cryoelectron tomography and pattern recognition. J. Struct. Biol. *156*, 334–341.

Rich, A. (1963). Polyribosomes. Sci. Am. *209*, 44–53.

Schuwirth, B.S., Borovinskaya, M.A., Hau, C.W., Zhang, W., Vila-Sanjurjo, A., Holton, J.M., and Cate, J.H. (2005). Structures of the bacterial ribosome at 3.5 Å resolution. Science *310*, 827–834.

Slayter, H., Kiho, Y., Hall, C., and Rich, A. (1968). An electron microscopic study of large bacterial polyribosomes. J. Cell Biol. *37*, 583–590.

Spirin, A.S. (2004). High-throughput cell-free systems for synthesis of functionally active proteins. Trends Biotechnol. *22*, 538–545.

Staehelin, T., Brinton, C.C., Wettstein, F.O., and Noll, H. (1963). Structure and function of E. coli ergosomes. Nature *199*, 865–870.

Tarun, S.Z., Jr., and Sachs, A.B. (1996). Association of the yeast poly(A) tail binding protein with translation initiation factor eIF-4G. EMBO J. *15*, 7168–7177.

Teter, S.A., Houry, W.A., Ang, D., Tradler, T., Rockabrand, D., Fischer, G., Blum, P., Georgopoulos, C., and Hartl, F.U. (1999). Polypeptide flux through bacterial Hsp70: DnaK cooperates with trigger factor in chaperoning nascent chains. Cell *97*, 755–765.

Tomic, S., Johnson, A.E., Hartl, F.U., and Etchells, S.A. (2006). Exploring the capacity of trigger factor to function as a shield for ribosome bound polypeptide chains. FEBS Lett. *580*, 72–76.

Valle, M., Zavialov, A., Li, W., Stagg, S.M., Sengupta, J., Nielsen, R.C., Nissen, P., Harvey, S.C., Ehrenberg, M., and Frank, J. (2003a). Incorporation of aminoacyl-tRNA into the ribosome as seen by cryo-electron microscopy. Nat. Struct. Biol. *10*, 899–906.

Valle, M., Zavialov, A., Sengupta, J., Rawat, U., Ehrenberg, M., and Frank, J. (2003b). Locking and unlocking of ribosomal motions. Cell *114*, 123–134.

Vanzi, F., Takagi, Y., Shuman, H., Cooperman, B.S., and Goldman, Y.E. (2005). Mechanical studies of single ribosome/mRNA complexes. Biophys. J. *89*, 1909–1919.

Warner, J.R., Rich, A., and Hall, C.E. (1962). Electron Microscope Studies of Ribosomal Clusters Synthesizing Hemoglobin. Science *138*, 1399–1403.

Wells, S.E., Hillner, P.E., Vale, R.D., and Sachs, A.B. (1998). Circularization of mRNA by eukaryotic translation initiation factors. Mol. Cell *2*, 135–140.

Wimberly, B.T., Brodersen, D.E., Clemons, W.M., Jr., Morgan-Warren, R.J., Carter, A.P., Vonrhein, C., Hartsch, T., and Ramakrishnan, V. (2000). Structure of the 30S ribosomal subunit. Nature *407*, 327–339.

Woolhead, C.A., McCormick, P.J., and Johnson, A.E. (2004). Nascent membrane and secretory proteins differ in FRET-detected folding far inside the ribosome and in their exposure to ribosomal proteins. Cell *116*, 725–736.

Yusupova, G., Jenner, L., Rees, B., Moras, D., and Yusupov, M. (2006). Structural basis for messenger RNA movement on the ribosome. Nature *444*, 391–394.